Title
Bi-layer silk fibroin grafts support functional tissue regeneration in a porcine model of onlay esophagoplasty

Journal
Journal of Tissue Engineering and Regenerative Medicine, 12(2)

ISSN
1932-6254

Authors
Algarrahi, Khalid
Franck, Debra
Cristofaro, Vivian
et al.

Publication Date
2018-02-01

DOI
10.1002/term.2402

Peer reviewed

HHS Public Access

Author manuscript

J Tissue Eng Regen Med. Author manuscript; available in PMC 2019 February 01.

Published in final edited form as:

J Tissue Eng Regen Med. 2018 February ; 12(2): e894–e904. doi:10.1002/term.2402.

Bi-layer Silk Fibroin Grafts Support Functional Tissue Regeneration in a Porcine Model of Onlay Esophagoplasty

Khalid Algarrahi[1,2], **Debra Franck**[1], **Vivian Cristofaro**[2,4,5], **Xuehui Yang**[1], **Alyssa Savarino**[1], **Saif Affas**[1,2], **Frank-Mattias Schäfer**[1], **Chiara Ghezzi**[3], **Russell Jennings**[2], **Arthur Nedder**[6], **David L. Kaplan**[3], **Maryrose P. Sullivan**[2,4,5], **Carlos R. Estrada Jr.**[1,2], and **Joshua R. Mauney**[1,2,§]

[1]Urological Diseases Research Center, Boston Children's Hospital, Boston, MA 02115, USA

[2]Department of Surgery, Harvard Medical School, Boston, MA 02115, USA

[3]Department of Biomedical Engineering, Tufts University, Medford, MA, 02155, USA

[4]Division of Urology, Veterans Affairs Boston Healthcare System, West Roxbury, MA 02132, USA

[5]Department of Surgery, Brigham and Women's Hospital, Boston, MA 02115, USA

[6]Animal Resource at Children's Hospital, Boston Children's Hospital, Boston, MA 02115, USA

Abstract

Partial circumferential, full thickness defects of the esophagus can occur as a result of organ perforation, tumor resection, or during surgical reconstruction of strictured segments. Complications associated with autologous tissue flaps conventionally utilized for defect repair necessitate the development of new graft options. In this study, bi-layer silk fibroin (BLSF) scaffolds were investigated for their potential to support functional restoration of partial circumferential defects in a porcine model of esophageal repair. Onlay thoracic esophagoplasty with BLSF matrices (~3 x 1.5 cm) was performed in adult swine (N=6) for 3 months of implantation. All animals receiving BLSF grafts survived with no complications and were capable of solid food consumption. Radiographic esophagrams revealed preservation of organ continuity with no evidence of contrast extravasation or strictures. Fluoroscopic analysis demonstrated peristaltic contractions. Ex vivo tissue bath studies displayed contractile responses to carbachol, electric field stimulation, and KCl while isoproterenol produced tissue relaxation. Histological and immunohistochemical evaluations of neotissues showed a stratified, squamous epithelium, a muscularis mucosa composed of smooth muscle bundles, and a muscularis externa organized into

[§]Corresponding author: Joshua R. Mauney, Ph.D., Boston Children's Hospital, Department of Urology, John F. Enders Research Laboratories, 300 Longwood Ave., Rm. 1009, Boston, MA 02115, USA; Phone: 617-919-2521; Fax: 617-730-0248; joshua.mauney@childrens.harvard.edu.

6. Conflict of interest

The authors declare no conflicts of interest.

7. Author Contributions

JRM, KA, AN, CRE, RJ, DLK designed and conceptualized this study. Acquisition of data was carried out by KA, DF, VC, XY, AS, SA, FMS, CG, and MPS. Analysis and interpretation of data was done by JRM, DF, VC, XY, AS, FMS, CG, and MPS. Manuscript was drafted by JRM, KA, DF, VC, MPS, while VC, MPS, RJ, CRE, and JRM performed critical revision of the manuscript for important intellectual content. Statistical analysis was done by KA, VC, and MPS. Funding was obtained by JRM, CRE, and DLK, and the entire study was supervised by JRM.

circular and longitudinal layers with a mix of striated skeletal muscle fascicles interspersed with smooth muscle. De novo innervation and vascularization were observed throughout the graft sites and consisted of synaptophysin positive neuronal boutons and vessels lined with CD31 positive endothelial cells. The results of this study demonstrate that BLSF scaffolds can facilitate constructive remodeling of partial circumferential, full thickness esophageal defects in a large animal model.

1. Introduction

Surgical reconstruction of partial circumferential, full thickness defects of the esophagus is often indicated during repair of benign strictures which are refractory to endoscopic dilatation (Raboei and Luoma 2008; Hugh *et al.,* 2008; Lin *et al.,* 2016) as well as in cases where tissue loss has occurred due to perforation (Richardson and Tobin, 1994; Benazzo *et al.,* 2008) or following tumor resection (Ki *et al.,* 2015). In these settings, onlay esophagoplasty with free or pedicled flaps derived from gastrointestinal, fasciocutaneous and myocutaneous tissues have been utilized to restore organ continuity and allow for transport of food and liquids (Mutton *et al.,* 1981; Hugh *et al.,* 1991; Noland *et al.,* 2011; Sa *et al.,* 2013; Lin *et al.,* 2016). Complications such as anastomotic leakage, stricture recurrence, diverticula, and graft necrosis have been reported with the use of these strategies (Kennedy *et al.,* 1995; Raboei and Luoma, 2008; Ki *et al.,* 2015), thus necessitating improved treatment modalities.

Over the past three decades, a number of acellular biodegradable biomaterials have been explored as alternatives to autologous tissue flaps for repair of partial circumferential, full thickness esophageal defects (Tan *et al.*, 2012). Patch grafts derived from decellularized tissues such as small intestinal submucosa and urinary bladder submucosa have been utilized for esophageal defect consolidation in a variety of preclinical animal models and short-term clinical trials (Badylak *et al.*, 2000; Lopes *et al.*, 2006a, 2006b; Urita *et al.,* 2007; Clough *et al.*, 2011; Nieponice *et al.*, 2014; Algarrahi *et al.*, 2015). However, suboptimal regenerative responses and complications such as scaffold leakage have been reported with these matrix designs, therefore raising doubts about their widespread translation into clinical settings (Urita *et al.,* 2007; Nieponice *et al.*, 2014; Algarrahi *et al.*, 2015). Meshes composed of synthetic polyesters have also demonstrated efficacy in supporting de novo tissue formation in large animal models of patch esophagoplasty (Aikawa *et al.*, 2013). Unfortunately, acidic byproducts of polyester degradation can lead to chronic inflammatory reactions in vivo (Ceonzo *et al.*, 2006) and thus increase the risk of implant failure from deleterious foreign body responses (Mauney *et al.*, 2011). These studies highlight the need to develop new acellular scaffold platforms for esophageal tissue engineering which can address the shortcomings with conventional implant formulations.

Clinically viable biomaterial configurations for patch esophagoplasty must possess optimal structural, mechanical and degradative characteristics sufficient to provide for initial defect reinforcement, but allow for gradual scaffold dissipation and subsequent constructive remodeling without eliciting adverse immune reactions. A recent study from our laboratory has shown that bi-layer silk fibroin (BLSF) matrices derived from *Bombyx mori* silkworm

cocoons exhibited such properties in a rat model of onlay esophagoplasty (Algarrahi *et al.*, 2015). This biodegradable scaffold design displays dual functionality during wound healing by providing a porous foam compartment permissive for host tissue integration while a buttressing film layer prevents leakage of luminal contents (Seth *et al.*, 2013). Specifically, the BLSF graft promoted constructive remodeling of esophageal defects with neotissues capable of contractile and relaxation functions sufficient to support solid food ingestion. Parallel assessments of BLSF scaffold performance with conventional SIS implants within the rodent defect model demonstrated significant advantages such as low immunogenicity, limited graft site contracture, and improved skeletal muscle formation and de novo innervation processes (Algarrahi *et al.*, 2015). In the present study, we investigated the ability of the BLSF matrix to support functional repair of partial circumferential, full thickness esophageal defects in swine in order to understand regenerative efficacy in an omnivore injury model with comparable anatomy to humans (Kapoor *et al.*, 2015).

2. Materials and Methods

2.1. Biomaterials

BLSF scaffolds were fabricated from aqueous silk fibroin solutions using a solvent-casting/salt-leaching process in combination with silk fibroin film casting as previously described (Seth *et al.*, 2013). BLSF scaffolds were steam autoclaved for sterilization and subjected to analytical or surgical procedures described below.

2.2. Mechanical testing

Scaffold specimens (N=18, ~3 cm^2) were subjected to uniaxial tensile evaluations to determine initial elastic modulus (EM), ultimate tensile strength (UTS) and % elongation to failure (ETF) using previously reported methodology (Algarrahi *et al.*, 2015) compliant with the American Society for Testing and Materials (ASTM) F2150-13 standard (ASTM, 2013) and specifically based on the D638-14 Test Method (ASTM, 2008).

2.3. Scanning electron microscopy (SEM)

BLSF scaffolds were air-dried overnight, sputtered coated with Pt/Pd and structural analysis was performed using a Zeiss scanning electron microscope, model EVO MA10 (Carl Zeiss AG, Germany) as previously reported (Tu *et al.*, 2013).

2.4. Onlay esophagoplasty porcine model

BLSF implants (N=6) were assessed in an onlay esophagoplasty model (Figure 1D–F) using adult Yucatan mini-swine (~35–65 kg, Coyote Consulting Company Inc., East Douglas, MA). Oral ingestion of food and water was restricted in all animals 12 h prior to surgery. Operative procedures were performed under sterile technique with maintenance anesthesia using 1–4% isoflurane following induction with intramuscular injection of 0.4 mg/kg atropine, 2.2 mg/kg xylazine, 4.4 mg/kg tiletamine+zolazepam. All swine were intubated and mechanically ventilated for the duration of the operative manipulations. A thoracic approach was utilized to access the esophagus through a right posterior lateral thoracotomy incision between the 7^{th} and 8^{th} intercostal space. Lung retraction was performed to uncover the posterior mediastinum and blunt dissection was carried out through the mediastinal

pleural to expose the esophagus. A full thickness, elliptical defect (~3 cm long and 1.5 cm wide) was created in the anterior esophageal wall 3 cm above the gastroesophageal junction via surgical tissue resection. The BLSF graft of equal size was incorporated into the defect site using interrupted 4-0 polyglactin sutures. Non-absorbable 4-0 polypropylene sutures were placed at the proximal, distal, and lateral edges of the anastomotic perimeter for identification of graft borders following animal harvest. In addition, 4-0 steel sutures were also positioned at the proximal/distal boundaries of the graft periphery for implant identification during radiographic analyses described below. Following these procedures, the esophagus was placed back into the posterior mediastinum and a chest tube was installed and connected to a Pleur-evac® chest drainage system (Teleflex, Morrisville, NC) to allow for lung expansion and prevention of a post-operative pneumothorax. The thoracotomy incision was subsequently suture closed and a 20 French MIC-KEY gastrostomy feeding tube (Kimberly-Clark, Franklin, MA) was then placed to allow for transient enteral feeding. The chest tube was removed 45 min thereafter once proper drainage of any fluid or air in thoracic cavity was achieved. Post-operative pain was managed with intramuscular injection of 1.1 mg/kg banamine immediately postoperatively and a transdermal 4 μg/kg fentanyl patch for 72 h.

Animals were sustained on enteral food slurry consisting of diluted pig feed mixed with PediaSure® (Abbott Laboratories, Columbus, OH) for 1 week post-op. Swine were then transitioned to oral feedings of standard pig feed over 48–72 h which was continued for the duration of the study. Animals were weighed and radiographic esophageal imaging was performed pre-operatively and at 1 week, 1, 2, and 3 month intervals post-operatively. Animals were euthanized at 3 months post scaffold implantation and tubular esophageal segments containing the original graft site and adjacent circumferential host tissue were axially dissected in half. Each segment (~1.5 cm in length) was further divided into equal circular rings containing either peripheral or central portions of the initial graft region. Both central and peripheral specimens were analyzed for ex vivo contractility/relaxation responses or subjected to histological, immunohistochemical (IHC), histomorphometric evaluations. For some outcome assessments, tubular esophageal segments excised 5 cm above the scaffold implantation site (proximal control) were analyzed in parallel. In addition, esophageal tissues isolated from nonsurgical (NS) control swine (N=7) were evaluated similarly for 3 month endpoint comparisons. All animal studies were approved by the Boston Children’s Hospital Animal Care and Use Committee prior to experimentation.

2.5. Radiologic imaging: Esophagrams and Fluoroscopy

Barium esophagram (N=6) and fluoroscopic (N=5) analyses were performed on swine receiving BLSF implants both pre-operatively and throughout the study period. A contrast agent (E-Z-EM® LIQUID E-Z-PAQUE Barium Sulfate suspension, E-Z-EM, Inc., NY) was instilled into the proximal esophagus through a stomach tube (Portex®, Jorgensen Laboratories, Inc. CO). Following contrast installation, lateral fluoroscopy was performed with an ADC/XRE Unicath SP fluoroscopy instrument (XRE Corporation, MA) and anterior/posterior (AP) and lateral esophagrams were acquired using an AMX-4 portable X-ray machine (General Electric, CT). Esophageal continuity, function, and the presence of

organ abnormalities such as strictures or fistulas were evaluated at the original graft sites demarcated with steel marking sutures.

2.6. Esophagoscopy

Flexible upper gastrointestinal endoscopy was executed on swine (N=2) repaired with BLSF scaffolds both pre-operatively and over the course of 2 months of implantation to assess temporal stages of graft remodeling. Animals were anesthetized by 1–4% isoflurane inhalation, intubated to prevent aspiration, and then placed on the left lateral position. A flexible endoscope (Olympus® GIF 130, Tokyo, Japan) was then advanced over the tongue and oropharynx to the esophageal graft site where the entire mucosal circumference was inspected. Images were acquired using an Olympus® video processor (Olympus® CV-100 video processor, Tokyo, Japan).

2.7. Ex vivo contractility and relaxation

Circular esophageal tissue specimens with and without mucosa from nonsurgical controls (N=7) and the BLSF implant group (N=6) at 3 months post-op were analyzed in tissue baths for ex vivo contractility responses to KCl (120 mM) and to carbachol (1 μM) as previously reported (Algarrahi *et al.*, 2015). In tissues pre-contracted with carbachol, maximum responses to electrical field stimulation (0.5–20 Hz, 0.5 ms pulse duration, 12 volts) were also measured during stimulation (on-contraction or -relaxation) and after stimulation (off-contraction). In addition, relaxation responses were determined in tissues pre-contracted with carbachol following administration with isoproterenol (10 μM).

2.8. Histological, immunohistochemical, and histomorphometric analyses

Following animal sacrifice, tubular esophageal specimens from control and implant regions were fixed in 10% neutral-buffered formalin, dehydrated in graded alcohols, and paraffin embedded. Five micron sections were stained with Masson's trichrome and Alcian blue (pH 2.5) using standard methods. IHC analyses were performed on specimens using the following primary antibodies: anti-slow skeletal myosin skeletal heavy (MYH) [Abcam, Cambridge, MA, 1:200 dilution], anti-α-smooth muscle actin (SMA) [Sigma-Aldrich, St. Louis, MO, 1:200 dilution], anti-pan-cytokeratin (CK) [Dako, Carpinteria, CA, 1:150 dilution], anti-CK4 [Abcam, 1:200 dilution], anti-CK14 [Abcam, 1:200 dilution], anti-filaggrin (FG) [Abcam, 1:200 dilution], anti-synaptophysin (SYP) [Abcam, 1:50 dilution], anti-CD31 [Abcam, 1:100 dilution], and anti-Ki67 [Abcam, 1:100 dilution]. Specimens were then stained with species-matched Alexa Fluor 488, 594, and 647-conjugated secondary antibodies (Thermo Fisher Scientific, Waltham, MA) while 4′, 6-diamidino-2-phenyllindole (DAPI) was used to counterstain nuclei. An Axioplan-2 microscope (Carl Zeiss MicroImaging, Thornwood, NY) was utilized for specimen visualization and representative fields were captured with Axiovision software (version 4.8).

Histomorphometric evaluations (N=6–7 animals per group) were executed on independent microscopic fields equally dispersed along the entire graft site and control regions using published methods (Chung *et al.*, 2014; Algarrahi *et al.*, 2015). Specifically, image thresholding and area measurements were acquired with ImageJ software (version 1.47) on 8 independent microscopic fields per tissue specimen (20X magnification) in order to

calculate the percentage of tissue area stained for MYH, α-SMA, and pan-CK per total field area examined. The number of SYP+ boutons were also quantified across 8 independent microscopic fields per tissue specimen (20X magnification) utilizing similar methods and normalized to total field area analyzed to determine density of synaptic transmission areas. The total number of CD31+ vessels was determined across 2 independent microscopic fields per tissue specimen (5X magnification) as described above and the mean vessel diameter in each field was calculated using ImageJ measurement tools.

2.9. Statistical analyses

Statistical analyses were performed with SPSS Statistics software v19.0 (http://www.spss.com) using the Kruskal-Wallis test in combination with the post-hoc Scheffé's method. Statistical significance was defined as $p<0.05$. Data were displayed as means ± standard deviation unless otherwise noted.

3. Results and Discussion

The structural components of the BLSF scaffold were characterized by SEM analysis (Figure 1A–C). The foam layer generated by solvent-casting/salt-leaching of the aqueous silk fibroin solution comprised the bulk of total matrix thickness (0.5 mm) and displayed relatively large pores (~400 μm diameter) interconnected by a network of small pores (~10 μm diameter) dispersed along the channels. A non porous silk fibroin layer (200 μm thick) was observed on the external face of the porous foam as a result of film annealing during casting. Prior to implantation, mean tensile properties of BLSF scaffolds were determined as UTS: 0.3±0.1 MPa; EM: 3.6±1.3 MPa; and ETF: 24.7±8.9%.

All six swine grafted with BLSF matrices survived until scheduled euthanasia at 3 months post implantation. No clinical signs of esophageal dysphasia, vomiting, or excessive salivation were observed at any point during the study period. All animals receiving BLSF scaffolds were capable of oral consumption of solid food following a 1 week period of enteral feeding. In addition, no significant weight loss was observed in swine at 3 months post scaffold implantation (48±14 kg) in comparison to pre-operative levels (46±13 kg). Radiographic esophagrams of reconstructed esophageal segments were similar to pre-operative assessments across all study time points with no features of contrast extravasation, strictures, fistulas, diverticula, or organ dilatation observed (Figure 2). Endoscopic evaluations at 1 week post-op revealed the presence of luminal scaffold fragments at the original graft site consistent with an ongoing stage of scaffold remodeling, however by 1 month post-op mucosal regeneration was observed within the implant region (Figure 3). Moreover, fluoroscopic analysis demonstrated prominent peristaltic contractions within the original graft site at 2 (see supporting information, Video_S1) and 3 months (see supporting information, Video_S2) post-op in all swine evaluated. Collectively, these data show the ability of BLSF scaffolds to support in situ esophageal function in a large animal model.

Gross tissue evaluations at 3 months post-op revealed host tissue ingrowth occupying the entire area of the original implantation site in all replicates with no evidence of luminal ulceration or significant axial or lateral contraction between marking sutures demarcating graft borders (Figure 4). Mild adhesions with the diaphragm were routinely observed on the

exterior of the graft walls. Global histological analyses of de novo esophageal tissues and controls revealed cross-sectional organization with distinct components consisting of a stratified, squamous epithelium; an ECM-rich, vascularized lamina propria; a muscularis mucosa populated with smooth muscle bundles, and a muscularis externa organized into circular and longitudinal layers containing a mixture of striated skeletal muscle fascicles interspersed with smooth muscle (Figures 5, 6A). In comparison to control specimens, the muscularis externa was qualitatively underdeveloped in the majority of neotissues, especially in the central graft regions, and presented as a discontinuous patchwork of muscular components with higher density toward the edges of the graft sites with respect to the interior. Future studies will investigate if longer periods of wound healing will lead to complete maturation of this compartment to baseline levels. Submucosal glands demonstrating Alcian blue positivity indicative of mucin production were observed in both experimental groups (Figure 6B). Scant residual scaffold fragments surrounded by focal points of putative macrophage phagocytosis were detected within the regenerating esophageal walls. Areas of mild fibrosis were apparent within the interior of the consolidated tissues, however chronic inflammatory reactions were not observed. Overall, our results show that BLSF scaffolds support constructive remodeling of partial circumferential esophageal defects without adverse immune reactions, however regeneration of the de novo muscularis externa was incomplete at the 3 month time point.

IHC (Figure 7) and histomorphometric (Figure 8) analyses were performed on experimental groups to ascertain the level of tissue maturation present at graft sites. Similar extents of pan-CK+ epithelia were observed in both nonsurgical controls as well as the central and peripheral regions of the neotissues. Moreover, epithelia in each group contained distinct epithelial subpopulations consisting of 1–2 layers of CK14+, Ki67+ basal cells, ~20 layers of polygonal CK4+ suprabasal cells, and 2–3 apical layers of flattened superficial cells displaying FG protein expression. In addition, no evidence of Alcian blue staining was detected in the de novo epithelial layers (data not shown) which is consistent with the absence of abnormal differentiation routinely seen in metaplastic conditions such as Barrett's esophagus (Irvanloo *et al.*, 2011). Proliferating host basal cells flanking the sites of scaffold anastomosis represent a putative progenitor cell population for the de novo epithelium given their role in epithelial repair in other injury models (Doupé *et al.*, 2012).

De novo innervation and vascularization processes were frequently observed throughout both peripheral and central regions of the neotissues. The density of SYP+ boutons representative of synaptic transmission regions were found to be similar across all regenerative areas in comparison to levels observed in nonsurgical controls. Vessels lined with CD31+ endothelial cells were present in all experimental groups. However, histomorphometric evaluations revealed that regenerated vascular networks displayed significantly lower mean vessel diameters with elevated mean vessel densities in respect to control levels. This pattern of vascularization is consistent with an ongoing stage of wound healing frequently observed in other tissue repair models wherein a large number of immature vessels initially invade defect sites while later some are pruned and the remaining vessels mature (Zawicki *et al.*, 1981; Jain, 2003).

Characterization of the regenerated muscularis mucosa at graft sites revealed the degree of α-SMA+ smooth muscle bundles in the peripheral and central regions had respectively achieved 65% and 75% of control levels by 3 months of implantation. Interestingly, the regenerated muscularis externa was found to contain significantly different amounts of α-SMA+ smooth muscle and MYH+ skeletal muscle in comparison to NS controls and esophageal segments isolated proximal to the reconstructed site. In particular, a 25–130 fold increase in the ratio of smooth (α-SMA+) to skeletal (MYH+) muscle was observed within the central (26) and peripheral (7.5) implant regions in respect to levels detected in nonsurgical (0.3) and proximal (0.2) tissues. This trend was specific to the implant site since the host tissue wall opposite the anastomotic site (wall-control) revealed a similar ratio (0.5) as observed in the other controls. These data are consistent with the results of Aikawa and colleagues which reported baseline elevations in smooth muscle content in the regenerating porcine muscularis externa over the course of implantation with a synthetic polymer graft (Aikawa *et al.*, 2013). In that study, the phenomenon was transient demonstrating a peak at 2 months post-op and gradual degradation by 3 months. Mechanisms governing muscle tissue regeneration in the adult esophagus are not largely understood. Lineage tracing studies in rodent models of esophageal development have concluded that separate progenitor populations are independently responsible for skeletal and smooth muscle formation and transdifferentiation between these lineages does not occur (Rishniw *et al.*, 2003, 2007, 2009). Our data support this notion in the setting of adult wound healing since no overlap between α-SMA and MYH expression was detected in any specimen examined. The increased presence of α-SMA+ smooth muscle observed in the muscularis externa during tissue remodeling may serve to temporarily support organ contractile function until baseline skeletal muscle has been restored; however this theory deserves further study.

Esophageal peristalsis is an essential function which involves symmetric contraction and relaxation of circular muscle in order to propel food bolus toward the stomach (Paterson, 2006). Functional evaluations of contractile behaviors in experimental groups were performed in ex vivo tissue bath studies following exposure to KCl and carbachol (Figure 9A, B). Regenerated tissues showed the ability to react to KCl thus demonstrating a functionally intact contractile machinery activated by membrane depolarization. Carbachol-induced contractile responses provided evidence that neotissues were capable of exhibiting muscarinic receptor-mediated effects on muscle physiology. Contractile responses were significantly augmented in both the central and peripheral implant regions in comparison to nonsurgical or proximal controls in response to both agonists tested. These results are potentially due to the higher proportion of smooth muscle observed in the graft regions in respect to control groups. Indeed, a previous study of the regional variations in the contractile response across the length of the feline esophagus demonstrated a positive correlation between smooth muscle content and the magnitude of agonist-induced force generation (Christensen and Dons, 1968). Parallel evaluations of experimental groups demonstrated prominent relaxation responses in carbachol-stimulated tissue rings following isoproterenol administration (Figure 9C). Contraction and relaxation responses were apparent in both denuded samples and those with intact mucosa, however tensile force was generally lower with an intact mucosa in all conditions examined. This feature is consistent with published reports demonstrating an inhibitory effect of the mucosa on the contractile

behaviors of esophageal tissues (Rieder *et al.*, 2010) and thus confirms the existence of this bioactivity in neotissues. Implant regions were highly reactive to electrical field stimulation, generating an enhanced relaxation response during stimulation (Figure 9D) and an augmented frequency dependent off-contraction compared to control tissues (Figure 9E). These responses indicate that excitatory and inhibitory neurotransmitters are released from functionally intact intrinsic enteric nerves in graft regions. During stimulation, the functional response is determined by a complex balance between enteric inhibitory nerves releasing nitric oxide and likely ATP, and excitatory nerves that release acetylcholine (Lecea *et al.*, 2012). The greater relaxation response during stimulation in regenerated tissues is consistent with decreased striated muscle content and extrinsic vagal innervation, and suggests a shift towards nitrergic innervation with tissue regeneration.

4. Conclusions

The results of this study demonstrate that acellular BLSF scaffolds were permissive for constructive remodeling of partial circumferential, full thickness defects in a porcine model of onlay esophagoplasty. Neotissues were composed of innervated, vascularized epithelial and muscular components which displayed contractile and relaxation responses sufficient to support organ peristalsis and solid food consumption. These matrices elicited minimal immune reactions and maintained the integrity of implantation sites with negligible contracture. BLSF grafts represent emerging options for the repair of functional esophageal tissues. Future preclinical evaluations will focus on investigating the potential of BLSF scaffolds to serve as tubular grafts for regeneration of full circumferential defects which are encountered in diseases such as esophageal atresia.

Supplementary Material

Refer to Web version on PubMed Central for supplementary material.

Acknowledgments

This research was supported by the Tissue Engineering Resource Center, NIH/NIBIB P41 EB002520 (DLK), BX001790 (MPS), and NIH/NIDDK R01 DK107568 (JRM). This research was also supported through the vision and generosity of the Rainmaker Group in honor of Dr. Alan Retik, MD. We also acknowledge Dr. Bryan Sack, MD and Mr. Kyle Costa BSc for technical support.

References

Aikawa M, Miyazawa M, Okamoto K, et al. A bioabsorbable polymer patch for the treatment of esophageal defect in a porcine model. J Gastroenterol. 2013; 48:822–829. [PubMed: 23229769]

Algarrahi K, Franck D, Ghezzi CE, et al. Acellular bi-layer silk fibroin scaffolds support functional tissue regeneration in a rat model of onlay esophagoplasty. Biomaterials. 2015; 53:149–159. [PubMed: 25890715]

ASTM D638–14. Standard Test Method For Tensile Properties Of Plastics. West Conshohocken, PA: American Society for Testing and Materials; 2008.

ASTM 2150–13. Standard Guide for Characterization and Testing of Biomaterial Scaffolds Used in Tissue-Engineered Medical Products. West Conshohocken, PA: American Society for Testing and Materials; 2013.

Badylak S, Meurling S, Chen M, et al. Resorbable bioscaffold for esophageal repair in a dog model. J Pediatr Surg. 2000; 35:1097–1103. [PubMed: 10917304]

Benazzo M, Spasiano R, Bertino G, et al. Sternocleidomastoid muscle flap in esophageal perforation repair after cervical spine surgery: concepts, techniques, and personal experience. J Spinal Disord Tech. 2008; 21:597–605. [PubMed: 19057255]

Ceonzo K, Gaynor A, Shaffer L, et al. Polyglycolic acid-induced inflammation: role of hydrolysis and resulting complement activation. Tissue Eng. 2006; 12:301–308. [PubMed: 16548688]

Christensen J, Dons RF. Regional variations in response of cat esophageal muscle to stimulation with drugs. J Pharmacol Exp Ther. 1968; 161:55–58. [PubMed: 5648502]

Chung YG, Algarrahi K, Franck D, et al. The use of bi-layer silk fibroin scaffolds and small intestinal submucosa matrices to support bladder tissue regeneration in a rat model of spinal cord injury. Biomaterials. 2014; 35:7452–7459. [PubMed: 24917031]

Clough A, Ball J, Smith GS, et al. Porcine small intestine submucosa matrix (Surgisis) for esophageal perforation. Ann Thorac Surg. 2011; 91:e15–6. [PubMed: 21256256]

Doupé DP, Alcolea MP, Roshan A, et al. A single progenitor population switches behavior to maintain and repair esophageal epithelium. Science. 2012; 337:1091–3. [PubMed: 22821983]

Hugh TB, Meagher AP, Li B. Gastric antral patch esophagoplasty for extensive corrosive stricture of the esophagus. World J Surg. 1991; 15:299–303. [PubMed: 2031367]

Irvanloo G, Fallahi B, Ensani F, et al. Endoscopic versus histological diagnosis of Barrett's esophagus: a cross-sectional survey. Pol J Pathol. 2011; 62:152–156. [PubMed: 22102072]

Jain RK. Molecular regulation of vessel maturation. Nat Med. 2003; 9:685–693. [PubMed: 12778167]

Kapoor H, Lohani KR, Lee TH, et al. Animal Models of Barrett's Esophagus and Esophageal Adenocarcinoma-Past, Present, and Future. Clin Transl Sci. 2015; 8:841–847. [PubMed: 26211420]

Kennedy AP, Cameron BH, McGill CW. Colon patch esophagoplasty for caustic esophageal stricture. J Pediatr Surg. 1995; 30:1242–1245. [PubMed: 7472994]

Ki SH, Choi JH, Sim SH. Reconstructive Trends in Post-Ablation Patients with Esophagus and Hypopharynx Defect. Arch Craniofac Surg. 2015; 16:105–113. [PubMed: 28913234]

Lecea B, Gallego D, Farré R, et al. Origin and modulation of circular smooth muscle layer contractions in the porcine esophagus. Neurogastroenterol Motil. 2012; 24:779–789. [PubMed: 22632463]

Lin YC, Hsiao JR, Lee YC. Patch esophagoplasty with a free proximal lateral leg flap for focal stricture of the cervical esophagus: A case report. Microsurgery. 2016 In Press.

Lopes MF, Cabrita A, Ilharco J, et al. Esophageal replacement in rat using porcine intestinal submucosa as a patch or a tube-shaped graft. Dis Esophagus. 2006a; 19:254–259. [PubMed: 16866856]

Lopes MF, Cabrita A, Ilharco J, et al. Grafts of porcine intestinal submucosa for repair of cervical and abdominal esophageal defects in the rat. J Invest Surg. 2006b; 9:105–111.

Mauney JR, Cannon GM, Lovett ML, et al. Evaluation of gel spun silk-based biomaterials in a murine model of bladder augmentation. Biomaterials. 2011; 32:808–818. [PubMed: 20951426]

Mutton T, Goco I, Pennell T. Management of esophageal perforation with a pedicled jejunal patch. Curr Surg. 1981; 38:318–321. [PubMed: 7297110]

Nieponice A, Ciotola FF, Nachman F, et al. Patch Esophagoplasty: Esophageal Reconstruction Using Biologic Scaffolds. Ann Thorac Surg. 2014; 97:283–288. [PubMed: 24266951]

Noland SS, Ingraham JM, Lee GK. The sternocleidomastoid myocutaneous "patch esophagoplasty" for cervical esophageal stricture. Microsurgery. 2011; 31:318–322. [PubMed: 21500276]

Paterson, WG. Esophageal peristalsis. Part 1 Oral cavity, pharynx and esophagus. In: Goyal, R., Shaker, R., editors. GI Motility Online. 2006.

Raboei EH, Luoma R. Colon patch esophagoplasty: an alternative to total esophagus replacement? Eur J Pediatr Surg. 2008; 18:230–232. [PubMed: 18629764]

Richardson JD, Tobin GR. Closure of esophageal defects with muscle flaps. Arch Surg. 1994; 129:541–547. [PubMed: 8185477]

Rieder F, Biancani P, Harnett K, et al. Inflammatory mediators in gastroesophageal reflux disease: impact on esophageal motility, fibrosis, and carcinogenesis. Am J Physiol Gastrointest Liver Physiol. 2010; 298:G571–G581. [PubMed: 20299604]

Rishniw M, Xin HB, Deng KY, et al. Skeletal myogenesis in the mouse esophagus does not occur through transdifferentiation. Genesis. 2003; 36:81–82. [PubMed: 12820168]

Rishniw M, Fisher PW, Doran RM, et al. Smooth muscle persists in the muscularis externa of developing and adult mouse esophagus. J Muscle Res Cell Motil. 2007; 28:153–165. [PubMed: 17638088]

Rishniw M, Fisher PJ, Doran RM, et al. Striated myogenesis and peristalsis in the fetal murine esophagus occur without cell migration or interstitial cells of Cajal. Cells Tissues Organs. 2009; 189:410–419. [PubMed: 18784410]

Sa YJ, Kim YD, Kim CK, et al. Recurrent cervical esophageal stenosis after colon conduit failure: use of myocutaneous flap. World J Gastroenterol. 2013; 19:307–310. [PubMed: 23345956]

Seth A, Chung YG, Gil ES, et al. The performance of silk scaffolds in a rat model of augmentation cystoplasty. Biomaterials. 2013; 34:4758–4765. [PubMed: 23545287]

Tan JY, Chua CK, Leong KF, et al. Esophageal tissue engineering: an in-depth review on scaffold design. Biotechnol Bioeng. 2012; 109:1–15. [PubMed: 21915849]

Tu DD, Chung YG, Gil ES, et al. Bladder tissue regeneration using acellular bi-layer silk scaffolds in a large animal model of augmentation cystoplasty. Biomaterials. 2013; 34:8681–8689. [PubMed: 23953839]

Urita Y, Komuro H, Chen G, et al. Regeneration of the esophagus using gastric acellular matrix: an experimental study in a rat model. Pediatr Surg Int. 2007; 23:21–26. [PubMed: 17004093]

Zawicki DF, Jain RK, Schmid-Schoenbein GW, et al. Dynamics of neovascularization in normal tissue. Microvasc Res. 1981; 21:27–47. [PubMed: 7010086]

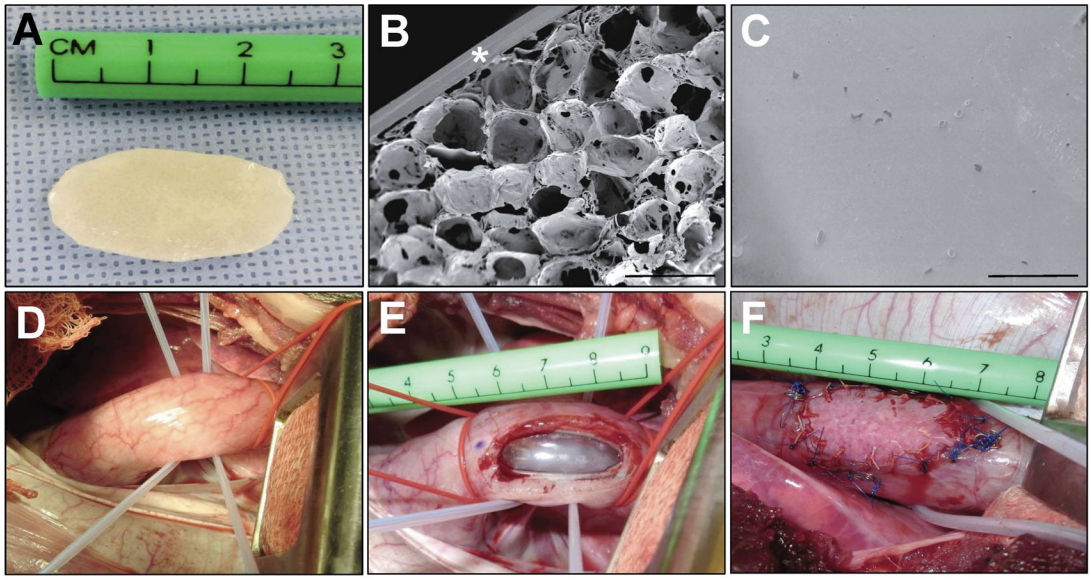

Figure 1.

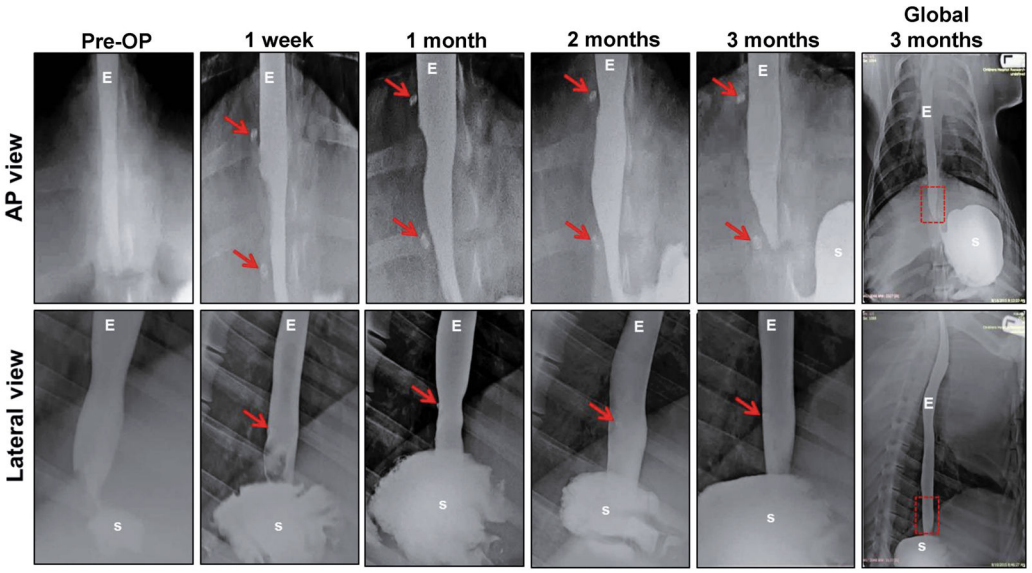

Figure 2.

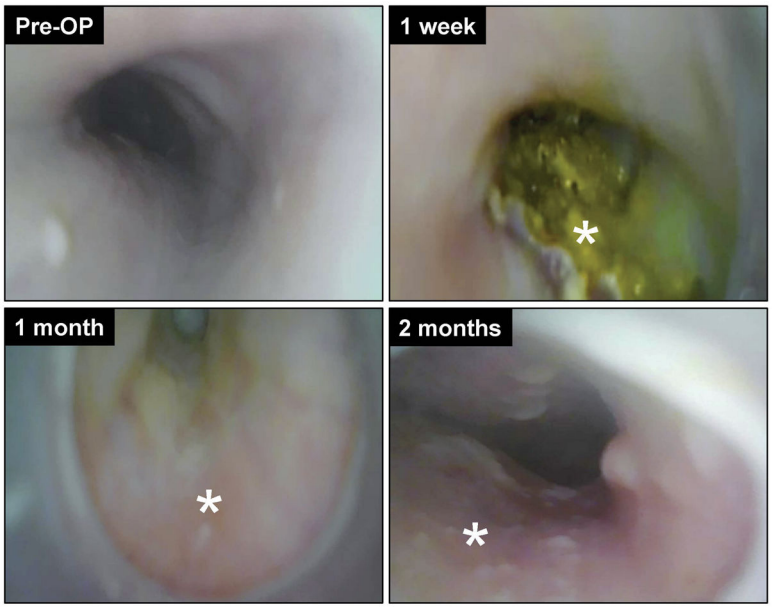

Figure 3.

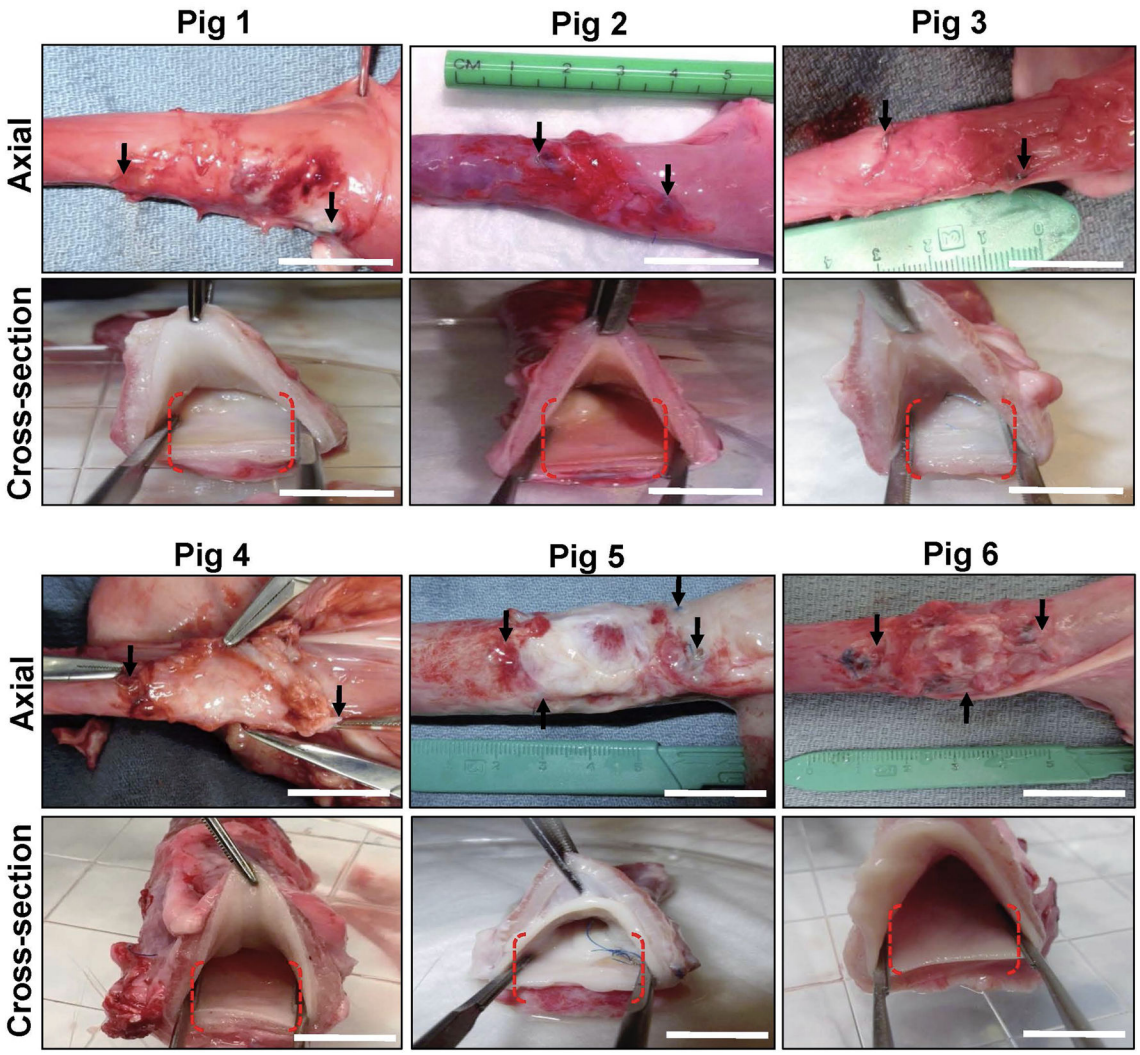

Figure 4.

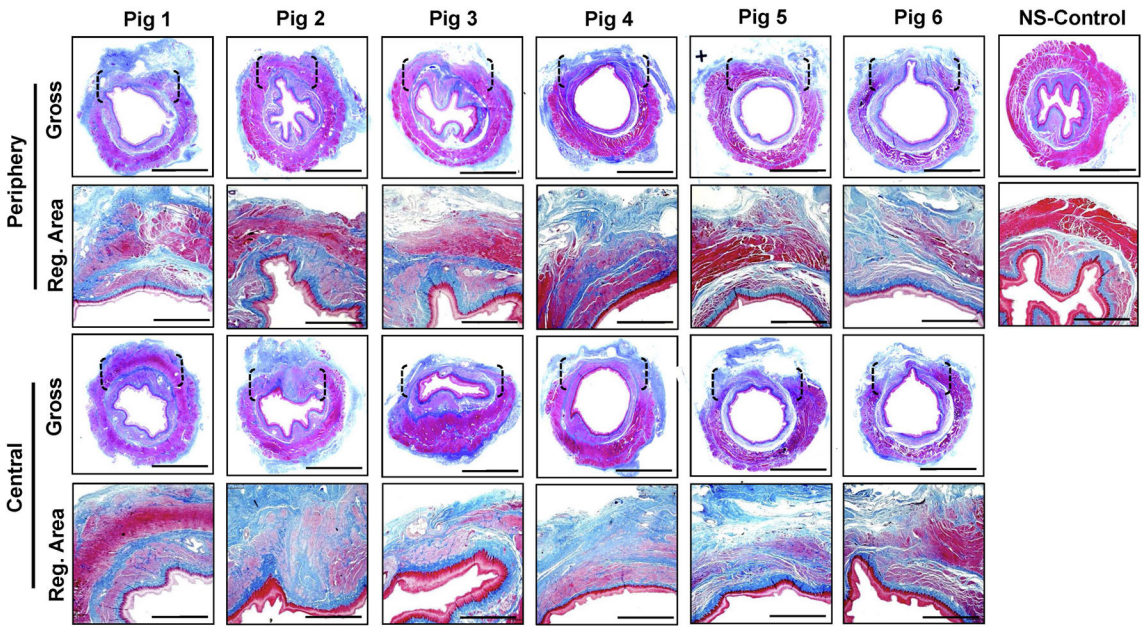

Figure 5.

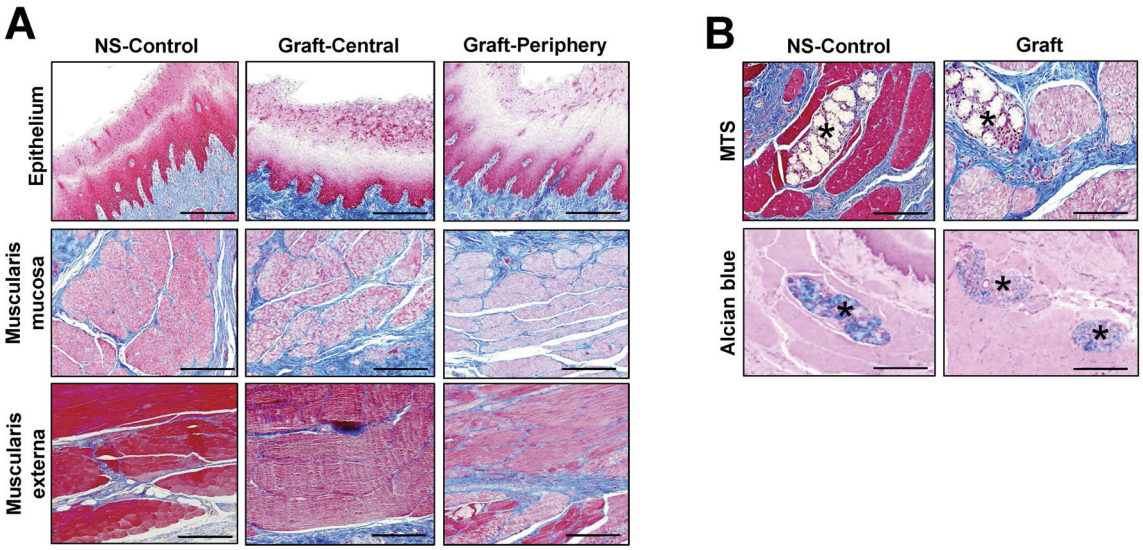

Figure 6.

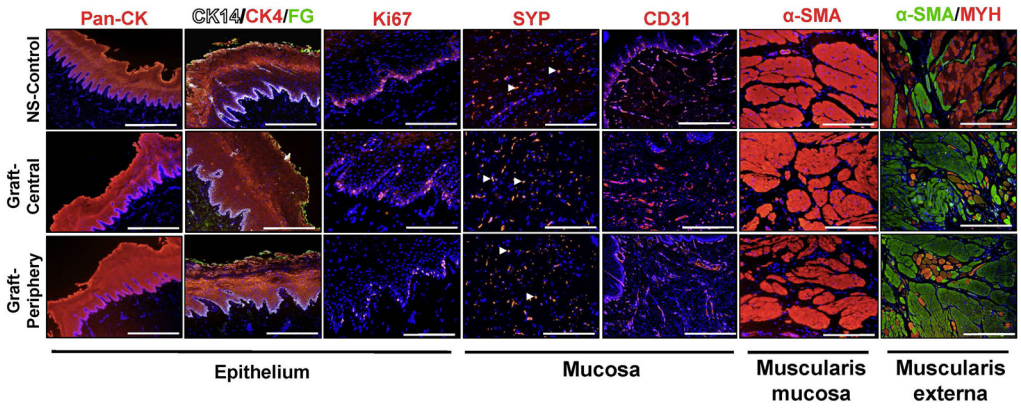

Figure 7.

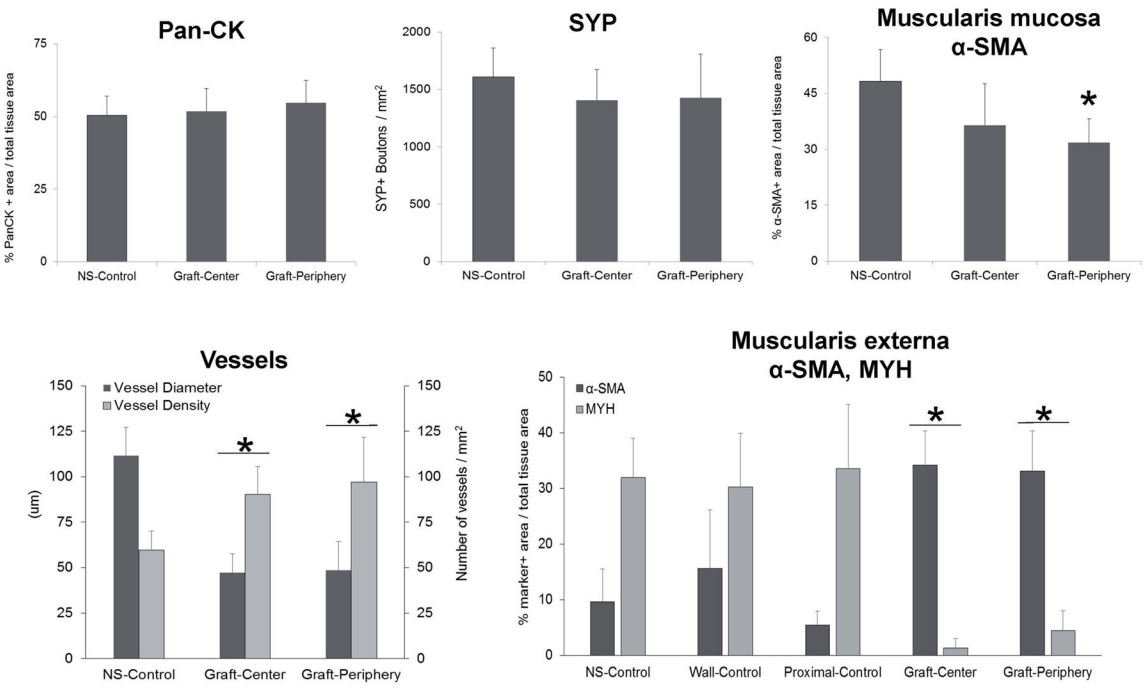

Figure 8.

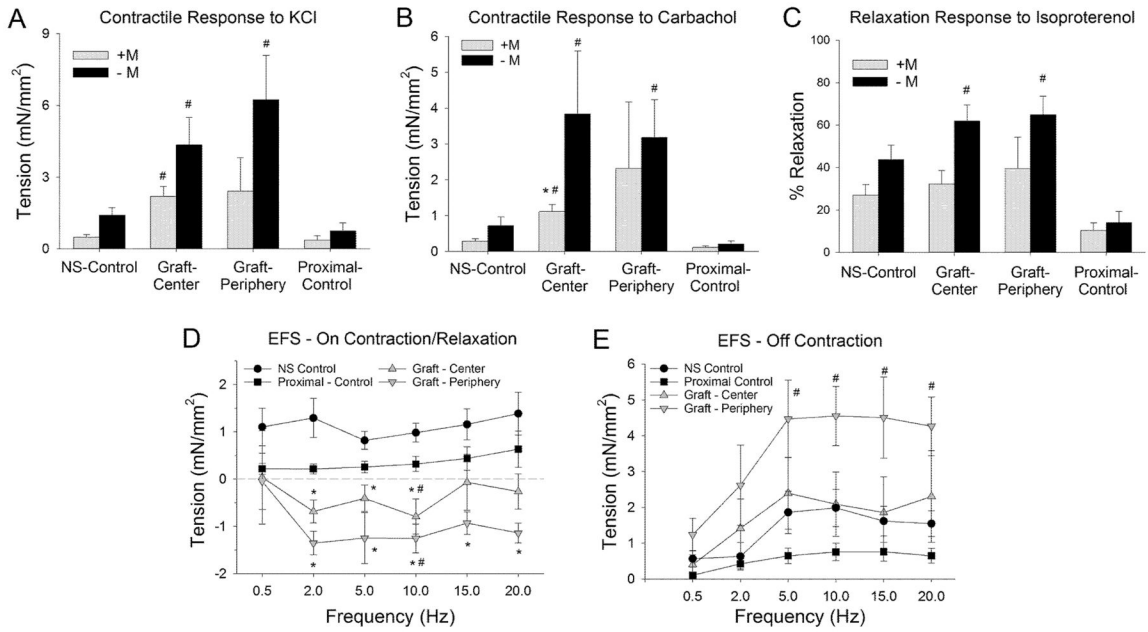

Figure 9.